The Astrophysical Journal Supplement Series, 154:75–79, 2004 September

SPITZER 24 MICRON OBSERVATIONS OF OPTICAL/NEAR-INFRARED–SELECTED EXTREMELY RED GALAXIES: EVIDENCE FOR ASSEMBLY OF MASSIVE GALAXIES AT $z \sim 1$–2?

Lin Yan,[1] Philip I. Choi,[1] D. Fadda,[1] F. R. Marleau,[1] B. T. Soifer[1,2] M. Im,[3] L. Armus,[1] D. T. Frayer,[1] L. J. Storrie-Lombardi,[1] D. J. Thompson,[2] H. I. Teplitz,[1] G. Helou,[1] P. N. Appleton,[1] S. Chapman,[2] F. Fan,[1] I. Heinrichsen,[1] M. Lacy,[1] D. L. Shupe,[1] G. K. Squires,[1] J. Surace, and G. Wilson[1]

Received 2004 April 5; accepted 2004 May 25

ABSTRACT

We carried out direct measurement of the fraction of dusty sources in a sample of extremely red galaxies with $(R - K_s) \geq 5.3$ mag and $K_s < 20.2$ mag, using 24 μm data from the *Spitzer Space Telescope*. Combining deep 24 μm K_s- and R-band data over an area of $\sim$64 arcmin^2 in ELAIS N1 of the *Spitzer* First Look Survey (FLS), we find that 50% $\pm$ 6% of our extremely red object (ERO) sample have measurable 24 μm flux above the 3 σ flux limit of 40 μJy. This flux limit corresponds to a star formation rate (SFR) of 12 $M_\odot$ yr^{-1} at $z \sim 1$, much more sensitive than any previous long-wavelength measurement. The 24 μm–detected EROs have 24 μm/2.2 μm and 24 μm/0.7 μm flux ratios consistent with infrared luminous, dusty sources at $z \geq 1$, and are an order of magnitude too red to be explained by an infrared quiescent spiral or a pure old stellar population at any redshift. Some of these 24 μm–detected EROs could be active galactic nuclei; however, the fraction among the whole ERO sample is probably small, 10%–20%, as suggested by deep X-ray observations as well as optical spectroscopy. Keck optical spectroscopy of a sample of similarly selected EROs in the FLS field suggests that most of the EROs in ELAIS N1 are probably at $z \sim 1$. The mean 24 μm flux (167 μJy) of the 24 μm–detected ERO sample roughly corresponds to the rest-frame 12 μm luminosity, $\nu L_\nu(12\ \mu\text{m})$, of $3 \times 10^{10}\ L_\odot$ at $z \sim 1$. Using the correlation between *IRAS* $\nu L_\nu(12\ \mu\text{m})$ and infrared luminosity $L_{\rm IR}(8\text{–}1000\ \mu\text{m})$, we infer that the $\langle L_{\rm IR} \rangle$ of the 24 μm– detected EROs is 3×10^{11} and $1 \times 10^{12}\ L_\odot$ at $z = 1.0$ and 1.5, respectively, similar to that of local luminous infrared galaxies (LIRGs) and ultraluminous infrared galaxies (ULIRGs). The corresponding SFR would be roughly 50–170 $M_\odot$ yr^{-1}. If the timescale of this starbursting phase is on the order of 10^8 yr as inferred for the local LIRGs and ULIRGs, the lower limit on the masses of these 24 μm–detected EROs is 5×10^9 to $2 \times 10^{10}\ M_\odot$. It is plausible that some of the starburst EROs are in the midst of a violent transformation to become massive early type galaxies at the epoch of $z \sim 1$–2.

Subject headings: galaxies: bulges — galaxies: evolution — galaxies: high-redshift — galaxies: starburst — infrared: galaxies

1. INTRODUCTION

Optical/near-infrared (NIR) colors such as $R - K_s$ or $I - K_s$ have been commonly used in wide-area surveys to select old stellar populations at $z \sim 1$–2 (see Cimatti et al. 2002; McCarthy et al. 2001; McCarthy 2004 for a review of this subject). NIR observations, which sample cool low-mass stars, are sensitive to old stellar populations. The $(R - K_s)$ of 5.3 mag corresponds to the calculated color of a passively evolving elliptical galaxy at $z = 1$. Therefore, in principle the color criterion of $(R - K_s) \geq 5.3$ mag or $I - K_s \geq 4$ mag (extremely red objects [EROs]) should select early-type galaxies at $z \sim 1$. However, these color selections are also sensitive to dust-reddened, star-forming systems, and examples of both passively evolving ellipticals and dusty starburst EROs have been found (Soifer et al. 1999; Hu & Ridgway 1994; McCarthy et al. 1992; Graham & Dey 1996). This indicates that the optical/NIR spectral energy distributions (SEDs) of these sources are sufficiently degenerate that these color criteria cannot effectively distinguish between them. In addition, a small fraction of EROs (10%–20%) could also be active galactic nuclei (AGNs), as shown by deep *Chandra* data and optical spectroscopy (Alexander et al. 2002; Yan et al. 2004). The relative contribution of these two galaxy types (old stellar populations and dust-reddened, star-forming galaxies) is a critical issue for many surveys whose goal is to determine the evolution of the mass function and the formation of massive galaxies. Deep optical spectroscopy indicates that a large fraction (30%–50%) of EROs have emission lines (Cimatti et al. 2002; Yan et al. 2004; McCarthy 2004); however, it remains unclear what fraction of EROs are truly dust-obscured galaxies.

Multiband Imaging Photometer for *Spitzer* (MIPS) 24 μm data from the *Spitzer Space Telescope* (Rieke et al. 2004; Werner et al. 2004) offer the first opportunity to directly address this critical issue. Dusty, star-forming galaxies are clearly distinguished from early type galaxies at mid-infrared (MIR) wavelengths. Between $z \sim 1$ and $z \sim 2$ the MIPS data is especially discriminating, since strong, rest-frame 6–12 μm polycyclic aromatic hydrocarbon (PAH) dust features redshift into the 24 μm band. In this paper, we present our initial study of the 24 μm properties of the $R - K_s \geq 5.3$ mag selected EROs in ELAIS N1. Throughout the paper, we adopt $H_0 = 70$ km s^{-1} Mpc^{-1}, $\Omega_M = 0.3$, $\Omega_\Lambda = 0.7$, and the Vega system for optical/NIR magnitudes.

2. DATA

2.1. *Spitzer* 24 μm *Observations and Data Reduction*

The primary data set used in this paper is in the ELAIS N1 field, which is a part of the *Spitzer* First Look Survey

[1] *Spitzer* Science Center, California Institute of Technology, 1200 East California Boulevard, MC 220-6, Pasadena, CA 91125; send offprint requests to Lin Yan at lyan@ipac.caltech.edu.

[2] Caltech Optical Observatories, California Institute of Technology, Pasadena, CA 91125.

[3] School of Earth and Environmental Sciences, Seoul National University, Shillim-dong, Kwanak-gu, Seoul, South Korea.

TABLE 1
SUMMARY OF OPTICAL, NIR, AND 24 μm OBSERVATIONS

Filter	FWHM (arcsec)	Pixel Scale (arcsec pixel^{-1})	⟨Exposure Time⟩ (s)	3 σ Limits (mag)
R.....	1.0	0.26	1800	25.5[a]/25.2[b]
K.....	1.0	0.25	1800[a]/9000[b]	20.3[a]/21.0[b]
24 μm.....	5.5	2.55	349[a]/4268[b]	90[a]/40[b,c]

[a] FLSV.
[b] ELAIS N1.
[c] In units of μJy.

(FLS).[4] The field was observed in a 2×2 pointing in photometry mode mosaic, and the raw data were processed and stacked by the data processing pipeline at the *Spitzer* Science Center (SSC). Source catalogs at 24 μm were generated using STARFINDER (Diolaiti et al. 2000), which measures profile-fitted fluxes for point sources. The complete description of the 24 μm data reduction and source catalog can be found in Marleau et al. (2004). To aid in the interpretation of the results from ELAIS N1, we also analyzed the FLS verification strip (FLSV). The data presented here covers 64 arcmin^2 in ELAIS N1 and 256 arcmin^2 in the FLSV. Table 1 summarizes the salient characteristics of all data used in this paper.

2.2. *Optical and NIR Imaging and Keck Spectroscopy*

All R-band observations were taken at the Kitt Peak National Observatory. Final stacked images and source catalogs have been publicly released (Fadda et al. 2004). The K_s-band data were obtained using the Wide-Field Infrared Camera (WIRC) on the Palomar 200 inch telescope. The K-band data in ELAIS N1 covers 8′×8′. A detailed description of the WIRC observations and data reduction are included in a separate paper by P. Choi et al. (2004, in preparation). Finally, high-resolution optical spectra of a K_s-selected galaxy sample within the FLS region were obtained using the Keck Deep Imaging Multi-object Spectrograph (DEIMOS; Faber et al. 2003). A total of ≈1000 redshifts were measured, of which 112 (52 EROs) are included in the analysis in this paper.

3. RESULTS AND IMPLICATIONS

3.1. *The* 24 μm*–Detected EROs*

To merge the R/K and 24 μm source catalogs, we used a simple positional matching method with a 2.″4 match radius, which corresponds to a 3 σ combined astrometric uncertainty from the K_s and 24 μm data. Because of the relatively low source density (7 arcmin^{-2}), the likelihood of spurious matches is small (3%), consistent with the fact that we find only one multiple match out of 65. In addition, we test the robustness of each match by comparing the probability of the measured separation based on the astrometric uncertainties to the probability of a spurious detection based on the 24 μm source density. The probability ratios above unity are implied to be likely real matches, and we found that all but two matches meet this criteria. We retained these two matches, since visual inspection suggests that they could still be associated with physical offset centroids. Bright stars were rejected using R-band images. Stellar contamination in our sample is expected to be small, since the field is at the Galactic latitude of 41°, and 24 μm data samples the tail of the Rayleigh-Jeans energy distribution.

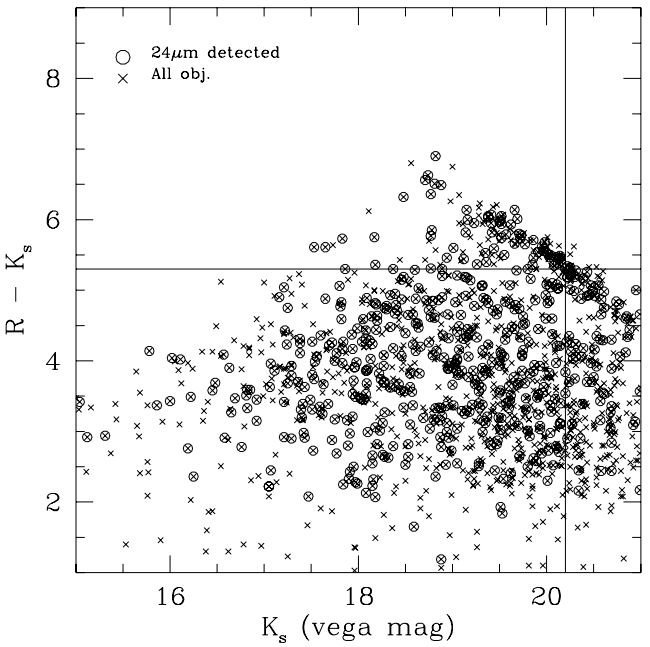

FIG. 1.—Color-magnitude diagram of $R - K_s$ vs. K_s. All K_s-band detected sources are shown as crosses, and sources with 24 μm counterparts are indicated by open circles. The $R - K_s \geq 5.3$ mag and $K_s < 20.2$ mag limits are shown as solid horizontal and vertical lines, respectively.

Since the R- and K_s-band data have similar seeing, $R - K_s$ colors were measured using a fixed 3″ diameter aperture. The ERO catalog with $R - K_s \geq 5.3$ mag and $K_s < 20.2$ mag (6 σ) consists of 129 galaxies over 64 arcmin^2 in ELAIS N1. Figure 1 shows the $R - K_s$ versus K_s distribution for all sources (*black crosses*). The $R - K_s \geq 5.3$ mag and $K_s < 20.2$ mag limits are shown as solid horizontal and solid vertical lines, and sources with 24 μm detected counterparts are indicated as red open circles. We find that 24 μm–detected sources have slightly redder $R - K_s$ colors than nondetected sources, consistent with the expectation that 24 μm emission is an indicator of dust extinction.

Of the 129 EROs, 65 (50% ± 6%) have 24 μm emission with flux greater than 40 μJy. The fraction of 24 μm–detected EROs becomes slightly higher for redder sources, with 56% ± 15% and 67% ± 30% for $R - K_s \geq 6.0$ mag and $R - K_s \geq 6.5$ mag, respectively. However, the errors of these fractions are large because of the shallow R-band limit. Deeper data are needed to reduce the uncertainties. In Figure 2*a*, we show the 24 μm flux distributions of both the total and ERO samples. We find that 70% of the 24 μm EROs have $f_{24\,\mu\mathrm{m}} > 90$ μJy and that the mean 24 μm flux of the ERO sample is 167 μJy. Figure 2*b* shows K_s versus 24 μm flux for all detected sources (*filled squares*) and for the EROs (*large open circles*). We find that among the 24 μm–detected sources, K_s is weakly correlated with $f_{24\,\mu\mathrm{m}}$, with large scatter. This is expected, since these two bands sample light from different physical origins, the stellar photosphere versus dust emission. This also explains why many faint K_s sources have fairly bright 24 μm fluxes. For

[4] For details of the FLS observation plan and the data release, see http://ssc.spitzer.caltech.edu/fls.

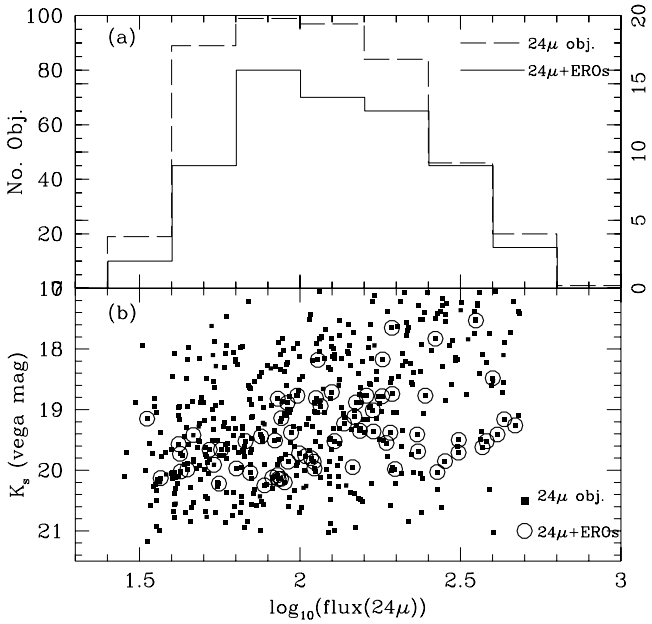

FIG. 2.—(*a*) 24 μm flux distribution of the total (*dashed line*) and 24 μm–detected ERO (*solid line*) populations. (*b*) K_s vs. 24 μm flux for all detected sources (*filled squares*) and for the EROs (*large open circles*).

K_s-bright ($\sim$18–17 mag) and 24 μm–faint sources, the MIR data is deep enough to detect the emission from normal galaxy populations at low redshifts.

3.2. *The Nature of the EROs with* 24 μm *Emission*

What types of galaxies are the 24 μm–detected EROs? In Figure 3*a* (Plate 1), we present a 24 μm/0.7 μm and 24 μm/2.2 μm color-color diagram showing that 24 μm–detected EROs (*red squares*) are clearly separated from EROs without 24 μm emission (*green*), as well as the general non-ERO population (*black and blue*). This suggests that the MIR/optical and MIR/NIR colors of 24 μm–detected EROs are unique, distinguishing them from other populations. Figure 3*b* presents the expected colors as a function of redshift for various SED templates, assuming no evolution. The SEDs for M51 (normal spiral), M82 (starburst), and Mrk 231 (dusty AGN) are taken from Silva et al. (1998), Fadda et al. (2002), and Chary & Elbaz (2001). In the case of M31's bulge (old stellar population), we use the NIR *J*, *H*, *K*, and *IRAS* 12, 25, 60, and 100 μm fluxes, all within a 4′ diameter aperture of the central nucleus (Soifer et al. 1986), and merge this with a 10 Gyr theoretical SED from Bruzual & Charlot.[5] For comparison, a sample of 112 24 μm sources from the FLSV with known spectroscopic redshifts are marked to show the actual redshift range of the 24 μm EROs in ELAIS N1. Of these 112 redshifts, 10 are 24 μm–detected EROs with $0.8 < z_{\rm spec} < 1.3$, and the optical spectra of these 10 sources all have a [O II] 3727 Å emission line.

Comparing Figure 3*a* and 3*b*, we reach the following conclusions:

1. 24 μm–detected EROs in ELAIS N1 with $R - K_s \geq 5.3$ mag, $K_s < 20.2$ mag, and $f_\nu(24\ \mu{\rm m}) > 40$ μJy are infrared-bright sources at $z \geq 1$. They have colors similar to starbursts such as M82 at $z \geq 1$, or dust reddened AGNs such as Mrk 231 at $z \geq 0.7$. Their colors are too red to be explained by any normal spiral or old stellar populations at any redshifts.

2. The likely redshift range of these 24 μm EROs is $z \geq 1$, as predicted from the model SEDs of M82 and Mrk 231. This is further confirmed by comparison with the Keck spectroscopic sample from the FLSV.

3. The remaining half of the ERO population are probably galaxies with old stellar populations at $z \sim 1$, as suggested by the tracks in Figure 3*b*.

Half of the ELAIS N1 ERO sample have 24 μm dust emission. The key question is what their infrared luminosities are. In the previous section, we conclude that the 24 μm–detected EROs have colors similar to M82; however, Figure 3*a* does not set any constraints on either their luminosities or masses. We have a total of 112 redshifts for objects with 24 μm counterparts (the FLSV 3 σ flux limit is 90 μJy). In Figure 4, we present the observed 24 μm luminosity versus redshift for the spectroscopic FLSV sample. At $z \sim 1$, the observed 24 μm luminosity roughly corresponds to the rest-frame *IRAS* 12 μm luminosity, within a factor of 2. The *Spitzer* 24 μm filter is narrower than the *IRAS* 12 μm filter, but ignoring this difference a crude conversion of the observed *Spitzer* 24 μm flux can be made to place a lower limit on the rest-frame *IRAS* 12 μm luminosity. We can infer the total infrared luminosity of 24 μm sources at $z \sim 1$ by using the correlation between the 12 μm luminosity, $\nu L_\nu(12\ \mu{\rm m})$, and the infrared luminosity $L_{\rm IR}(8-1000\ \mu{\rm m})$, $L_{\rm IR} = 0.89[\nu L_\nu(12\ \mu{\rm m})]^{1.094}\ L_\odot$ (Soifer et al. 1989; Chary & Elbaz 2001). The mean flux (167 μJy) of the 24 μm–detected EROs in ELAIS N1 implies $L_{\rm IR} \sim 3\times10^{11}\ L_\odot$ at $z = 1.0$ and $L_{\rm IR} \sim 10^{12}\ L_\odot$ at $z = 1.5$, similar to that of local LIRGs and ULIRGs. The corresponding SFR is 50–170 $M_\odot$ yr^{-1}, using ${\rm SFR} = 1.71\times10^{-10}\ L_{\rm IR}$ ($M_\odot$ yr^{-1}) (Kennicutt 1999). We emphasize that the 3 σ flux limit of 40 μJy in ELAIS N1 corresponds to a SFR of 12 $M_\odot$ yr^{-1}, more sensitive than the deepest 1.4 GHz observation (Smail et al. 2002). In comparison, the SFR derived from the rest-frame [O II] λ3727 emission line for EROs is roughly a few $M_\odot$ yr^{-1} (Yan et al. 2004; Cimatti et al. 2002). Our results are consistent with very deep 1.4 GHz (rms $\sim$ 3 μJy) measurements (Smail et al. 2002).

3.3. *Summary and Implications*

Spitzer 24 μm data in ELAIS N1 have revealed that 50% $\pm$ 6% of EROs with $R - K_s \geq 5.3$ mag and $K_s < 20.2$ mag have detectable 24 μm emission above 40 μJy. The colors and inferred redshifts of the 24 μm–detected EROs suggest that they are infrared-luminous, dusty sources at $z \geq 1$. Their mean 24 μm flux (167 μJy) corresponds to $\langle L_{\rm IR}\rangle \sim 3\times10^{11}\ L_\odot$ at $z \sim 1$ and to $\langle L_{\rm IR}\rangle \sim 10^{12}\ L_\odot$ at $z \sim 1.5$. Some of these 24 μm–detected EROs could be AGNs. The 1 Ms *Chandra* observation in the Hubble Deep Field and optical spectroscopy suggest that the fraction of EROs likely to be AGNs is small, around 10%–20% (Alexander et al. 2002; Yan et al. 2004). These dusty AGNs can be identified when we combine this current analysis with the Infrared Array Camera (IRAC) data. Our result suggests that a significant fraction of EROs are extremely active starbursts (LIRGs or ULIRGs). If the timescale of this starbursting phase is on the order of 10^8 yr^{-1}, as inferred from local LIRGs and ULIRGs (Sanders & Mirabel 1996), we can set a lower limit to the mass of these 24 μm–detected EROs as ${\rm SFR}\times\tau = (50\times10^8) - (170\times10^8) = (5\times10^9) - (2\times10^{10})\ M_\odot$. If the EROs *without* detectable 24 μm are indeed massive systems with old stellar populations at $z \sim 1$ as measured by several recent surveys (Glazebrook et al. 2004;

[5] The Bruzual & Charlot model is available at ftp://gemini.tuc.noao.edu/pub/charlot/bc95.

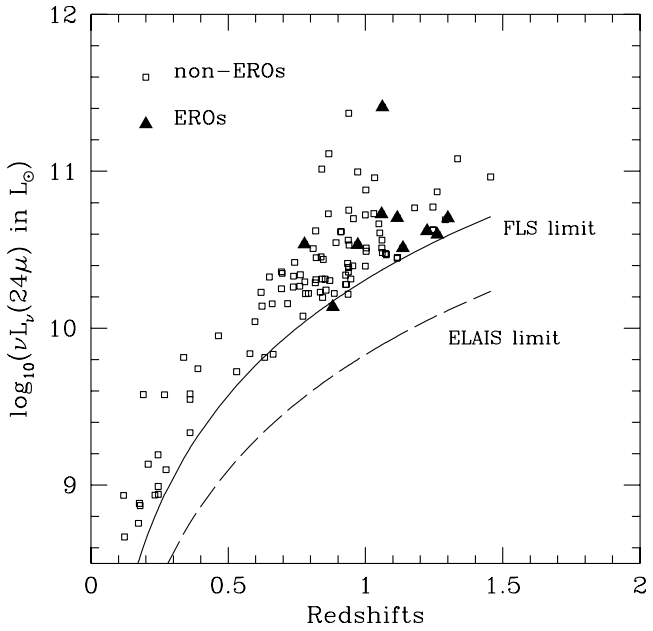

FIG. 4.—Observed 24 μm luminosity as a function of spectroscopic redshift for a sample of 112 24 μm–detected sources in the FLSV region. The solid triangles are 24 μm–detected EROs.

Bell et al. 2003), one plausible connection between the starburst and early-type ERO populations is that the former may be in the process of transforming into the latter, as initially postulated by Kormendy & Sanders (1992). In the hierarchical clustering paradigm, it could be interpreted that our deep 24 μm observations are capturing a massive galaxy population in the midst of violent transformation, possibly in the process of assembly via mergers/starbursts at the epoch of $z \sim 1-2$. The accurate determination of the stellar and dynamical masses of these starburst EROs at $z \sim 1-2$ will be critical for the resolution of this question. Finally, the measurement of volume-averaged mass density at $z \sim 1-2$ would require a better understanding of the physical source of the integrated K-band light, whether from dusty systems or from old stars.

Our result is consistent with what has been found with *Hubble Space Telescope* (*HST*) morphological studies of EROs. Yan & Thompson (2003) and Moustakas et al. (2004) have found that close to 50% of EROs with $K_s < 20$ mag have morphologies consistent with disk or later type galaxies in the observed 8100–8500 Å wavelength, and less than 40% show clean bulge-type profiles. With the *HST* ACS/NICMOS images in the FLSV region, we will be able to investigate the morphologies of these infrared luminous EROs, and to determine if indeed they are starbursting mergers at $z \sim 1$.

This work is based in part on observations made with the *Spitzer Space Telescope*, which is operated by the Jet Propulsion Laboratory, California Institute of Technology, under NASA contract 1407. Support for this work was provided by NASA. The spectroscopic data presented herein were obtained at the W. M. Keck Observatory, which is operated as a scientific partnership among the California Institute of Technology, the University of California, and the National Aeronautics and Space Administration. The Observatory was made possible by the generous financial support of the W. M. Keck Foundation. We also wish to recognize and acknowledge the very significant cultural role and reverence that the summit of Mauna Kea has always had within the indigenous Hawaiian community. We are most fortunate to have the opportunity to conduct observations from this mountain.

REFERENCES

Alexander, D. M., Vignali, C., Bauer, F. E., Brandt, F. E., Hornschemeier, A. E., Garmire, G. P., & Schneider, D. P. 2002, AJ, 123, 1149
Bell, E. F., McIntosh, D. H., Katz, N., & Weinberg, M. D. 2003, ApJS, 149, 289
Diolaiti, E., Bendinelli, O., Bonaccini, D., Close, L., Currie, D., & Parmeggiani, G. 2000, A&AS, 147, 335
Chary, R., & Elbaz, D. 2001, ApJ, 556, 562
Cimatti, A., et al. 2002, A&A, 381, L68
Faber, S. M., et al. 2003, Proc. SPIE, 4841, 1657
Fadda, D., Jannuzi, B., Ford, A., & Storrie-Lombardi, L. J., 2004, AJ, 128, 1
Fadda, D., et al. 2002, A&A, 383, 838
Glazebrook, K., et al. 2004, Nature, 430, 181
Graham, J., & Dey, A. 1996, ApJ, 471, 720
Hu, E. M., & Ridgway, S. E. 1994, AJ, 107, 1303
Kennicutt, R. C. 1999, ARA&A, 36, 189
Kormendy, J., & Sanders, D. 1992, ApJ, 390, L53
Marleau, F., et al. 2004, ApJS, 154, 66
McCarthy, P. J. 2004, ARA&A, 2004, submitted
McCarthy, P. J., Persson, S. E., & West, S. C. 1992, ApJ, 386, 52
McCarthy, P. J., et al. 2001, ApJ, 560, L131
Moustakas, L., et al. 2004, ApJ, 600, L131
Rieke, G., et al. 2004, ApJS, 154, 25
Sanders, D., & Mirabel, I. F. 1996, ARA&A, 34, 749
Silva, L., Granato, G. L., Bressan, A., & Danese, L. 1998, ApJ, 509, 103
Smail, I., Owen, F. N., Morrison, G. E., Keel, W. C., Ivison, R. J., & Ledlow, M. J. 2002, ApJ, 581, 844
Soifer, B. T., Boehmer, L., Neugebauer, G., & Sanders, D. B. 1989, AJ, 98, 766
Soifer, B. T., Matthews, K., Neugebauer, G., Armus, L., Cohen, J. G., Persson, S. E., & Smail, I. 1999, AJ, 118, 2065
Soifer, B. T., Rice, W. L., Mould, J. R., Gillett, F. C., Rowan-Robinson, M., & Habing, H. J. 1986, ApJ, 304, 651
Werner, M., et al. 2004, ApJS, 154, 1
Yan, L., & Thompson, D. J. 2003, ApJ, 586, 765
Yan, L., Thompson, D. J., & Soifer, B. T. 2004, AJ, 127, 1274

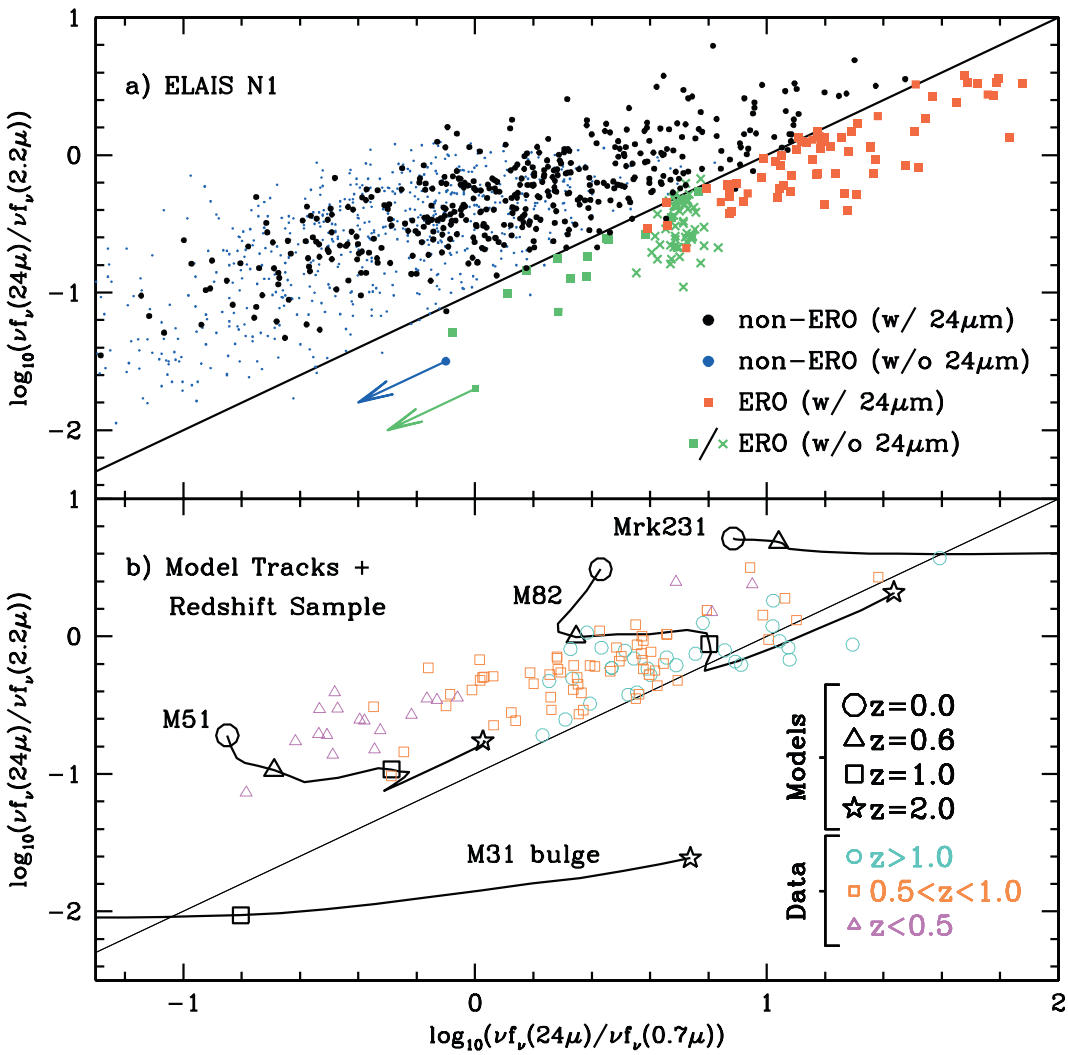

FIG. 3.—Plots of $\log_{10}[\nu f_\nu(24\ \mu\mathrm{m})/\nu f_\nu(0.7\ \mu\mathrm{m})]$ vs. $\log_{10}[\nu f_\nu(24\ \mu\mathrm{m})/\nu f_\nu(8\ \mu\mathrm{m})]$. (*a*) Data from ELAIS N1. In this panel, red and green squares represent EROs with and without 24 μm detections, respectively. For the non–24 μm EROs, the green crosses have only upper limits in the *R* band. The black and blue points represent the full K_s-selected sample with and without 24 μm detections, respectively. The plotted colors of sources not detected at 24 μm are upper limits and could move down to the lower right corner of the diagram, as illustrated by the green and blue arrows. The black solid line in both panels represents constant $R - K_s = 5.3$ mag color. (*b*) Computed color-color tracks as a function of redshift for a set of SED templates of local, well-known galaxies. The subset of the FLSV sample with measured spectroscopic redshifts are overplotted for three different redshift bins: $z < 0.5$ (*magenta open triangles*), $0.5 < z < 1.0$ (*orange open squares*), and $z > 1.0$ (*cyan open circles*).